Sustainable Energy & Fuels

Methanesulfonic Acid-based Electrode-decoupled Vanadium-Cerium Redox Flow Battery Exhibits Significantly Improved Capacity and Cycle Life

Journal:	*Sustainable Energy & Fuels*
Manuscript ID	SE-ART-05-2019-000286.R1
Article Type:	Paper
Date Submitted by the Author:	14-Jun-2019
Complete List of Authors:	Sankarasubramanian, Shrihari; Washington University in St. Louis, Energy, Environment and Chemical Engineering Zhang, Yunzhu; Washington University in Saint Louis, Energy, Environmental and Chemical Engineering Ramani, Vijay; Washington University in St. Louis, Energy, Environment and Chemical Engineering

Methanesulfonic Acid-based Electrode-decoupled Vanadium-Cerium Redox Flow Battery Exhibits Significantly Improved Capacity and Cycle Life

Shrihari Sankarasubramanian, Yunzhu Zhang, Vijay Ramani[z]

Center for Solar Energy and Energy Storage, Department of Energy, Environmental and Chemical Engineering, Washington University in St. Louis, One Brookings Dr., St. Louis, MO 63130, USA

[z] Corresponding Author's email: ramani@wustl.edu

Abstract

An electrode-decoupled V-Ce redox flow battery (ED-RFB) was developed with 40% greater theoretical volumetric capacity and a 30% enhancement in practical volumetric capacity was demonstrated. The use of methanesulfonic acid supported V and Ce electrolytes and a highly permselective polystyrene-block-poly(ethylene-ran-butylene)-block-polystyrene (SEBS) triblock copolymer anion exchange separator enabled a >95% reduction in capacity fade compared to standard H_2SO_4 supported V-Ce ED-RFBs. The methanesulfonic acid supported V and Ce electrolytes was examined using the Marcus-Hush kinetic formulation and the presence of strongly solvated cations was shown to reduce capacity fade by cation cross-over. The ED-RFB maintained nearly 100% coulombic efficiency (CE) and *ca.* 70% energy efficiency (EE) (at a 50 $mA.cm^{-2}$ galvanostatic charge/discharge current) over 100 cycles. The EE ranged from 85% at 25 $mA.cm^{-2}$ to 50% at 100 $mA.cm^{-2}$. The separator was highly acid stable with no changes in its FT-IR spectra and ionic conductivity before and after cycling. Thus, a V-Ce ED-RFB with long life, excellent rate capability and stability is demonstrated. The use of CH_3SO_3H, a "green" chemical with low toxicity and easy effluent treatment, facilitates scale-up and grid-scale deployment.

Introduction

The need to ensure the reliability and resiliency of the grid is greater than ever due to the market-driven increase in the penetration of intermittent renewable energy sources[1,2]. Grid-scale energy storage systems such as redox flow batteries (RFBs) are excellent candidates for this application[3]. RFBs are a special class of electrochemical energy storage system where the electroactive materials are stored outside the cell or battery itself. This arrangement decouples the energy and power obtainable from a given unit as the energy is a function of the amount of externally stored electroactive material while the power is a function of the stack size and chosen electroactive materials. This in turn ensures that the cost of these systems scale sub-linearly[4,5].

RFBs have been extensively investigated over the past forty years with the Fe-Cr[6–8], all-V[9,10], Zn-Ce[11–13] and all-Fe[14,15] chemistries being the subject of substantial research focus. The challenges have been bringing down the cost, reducing side reactions and (in case of chemistries where plating is involved) to addressing dendrite-driven failure modes. More recently, aqueous RFBs with organic electrolytes[16–19] and non-aqueous RFBs[20–23] have been investigated. These studies typically claim substantial cost savings (upon eventual mass-production of the demonstrated lab-scale actives) while achieving improved performance and stability. A key challenge in these systems is to ensure long lifetime (in the 10s of years) by minimizing capacity fade. A major cause of capacity fade is the mixing of the anolyte and catholyte with half the dissolved actives being rendered inactive at the anode and cathode respectively. Possible solutions to this issue include the use of elemental actives soluble at multiple oxidation state (such as V), equimolar anolyte-catholyte solutions as electrolytes (sacrificing 50% of theoretical volumetric capacity) or the use of large redox active molecules in conjunction with size-selective separators. The use of a highly permselective anion exchange membrane (AEM) as the separator eliminates

all the above restrictive conditions. A much broader ranges of elemental active species can be used in an electrode-decoupled manner (i.e. different cationic actives at the catholyte and anolyte) without mixing based capacity fade.

The chemistry that is farthest along in terms of commercialization is the all-V RFB. The all-V RFB eliminates mixing based capacity fade modes by utilizing different oxidation states of vanadium at the anode and cathode (allowing for the use of cation exchange membrane separators). The redox potentials of the vanadium couples used ensure a >1 V cell voltage and no significant hydrogen evolution or oxygen evolution reactions. The electrode reactions of an all-V RFB are as follows –

$$V^{3+} + e^- \leftrightarrow V^{2+} \ (E^0 = -0.26 \text{ V}) \quad (1)$$

$$VO^{2+} + e^- \leftrightarrow VO_2^+ \ (E^0 = 1.00 \text{ V}) \quad (2)$$

The high cost of vanadium[4], the relatively low cell voltage and the VO_2^+ induced degradation of the membrane separators[24] are all major disadvantages of this system. We have previously addressed these issues by demonstrating anion exchange membrane separator based V-Ce RFBs that are electrode-decoupled (i.e. ideally no mixing of anolyte and catholyte) with a theoretical OCV of 1.87 V by replacing the VO^{2+}/VO_2^+ couple with the Ce^{3+}/Ce^{4+} couple[25,26] (schematic in **Figure 1**). The Ce^{3+}/Ce^{4+} redox reaction is as follows –

$$Ce^{4+} + e^- \leftrightarrow Ce^{3+} \ (E^0 = 1.61 \text{ V}) \quad (3)$$

The major drawback of these batteries is that the Ce electrolyte has a relatively low solubility of 0.5 M in the typical H_2SO_4 supporting electrolyte[27] leading to a maximum theoretical volumetric capacity of 13.4 $Ah.L^{-1}$. The present study addresses this problem by reformulating the electrolyte using methanesulfonic acid as the supporting electrolyte. This is the first study, to the best of our

knowledge, to demonstrate an electrode-decoupled V-Ce system with methanesulfonic acid-based electrolytes on both the V and Ce sides.

Ce electrolytes with methanesulfonic acid as the supporting electrolyte have been previously employed in other Ce RFBs such as the Zn-Ce[11,12,29,30] and Pb-Ce[31] systems. Leung *et. al.*[32] reports a mixed sulfuric acid-methanesulfonic acid supported V-Ce RFB where a cation exchange membrane (CEM) separator is employed, inevitably leading to cation cross-over and capacity fade. The resultant drastic capacity fade is a possible reason for no long-term cycling data being reported in Leung *et. al.*[32]. Govindan *et. al.*[33] demonstrated a V-Ce system using H_2SO_4 supported V electrolyte and a CH_3SO_3H supporting Ce electrolyte. Similar to Leung *et. al.*[32], this report also employs a CEM that readily permits cation cross-over. Further, the electrolyte formulation with different acids on across the membrane will lead to osmotic pressure differences that exacerbate cation cross-over. This explains the *ca.* 50% capacity fade within 3 cycles reported in that paper, rendering their system highly impractical for energy storage over the decadal timescales. The present study addresses these issues and reduces capacity fade to 2.4% over 100 cycles.

The present study reports the use of methanesulfonic acid supported Ce and V electrolytes separated by an AEM that enables true electrode decoupled RFB operation. The key innovation of using the highly selective polystyrene-block-poly(ethylene-ran-butylene)-block-polystyrene (SEBS) triblock copolymer separators and the bulkier nature of the methanesulfonate coordinated ions ensured minimal cross-over and enabled us to demonstrate minimal capacity fade over 100 charge-discharge cycles (0.024% capacity fade per cycle). The membranes were chemically stable in both the V and Ce ions and the methanesulfonic acid. The use of methanesulfonic acid as the supporting electrolyte, balancing the inverse relationship between Ce^{3+} and Ce^{4+} solubilities with

increasing CH_3SO_3H concentrations[27], enabled electrolyte concentrations of up to 1M at room temperature. Having limited the concentration to 0.9 M to prevent precipitation due to local concentration variations, we demonstrate a V-Ce electrode-decoupled (ED-) RFB with 30% higher practical capacity than previous reports. Methanesulfonic acid confers the added benefit of using a "green" chemical with low relative toxicity and ease of disposal[34]. Thus, a high-performance ED-RFB has been developed.

Experimental

Synthesis and characterization of anion exchange separators

The polystyrene-block-poly(ethylene-ran-butylene)-block-polystyrene (SEBS) triblock copolymer separators with 30 % wt. of styrene were synthesized as described by us previously in Wang et al.[26,35] ,characterized using methods described therein, and the physical properties were found to closely match the previous report. The AEMs were initially prepared in the chloride form and then ion exchanged by immersion in 0.1M H_2SO_4 or 0.1M CH_3SO_3H to produce the sulfate or methanesulfonate forms respectively. The stability of the AEMs was characterized by immersing them in 4 M CH3SO3H at 40 ℃ for 5 weeks and periodically measuring the change (if any) in ionic conductivity and ion exchange capacity (IEC). The cross-sectional scanning electron microscopy (SEM) of the membrane was carried out using a FEI Nova NanoSEM 230 scanning electron microscope (SEM) with an attached energy dispersive analysis of X-rays (EDAX) detector. The Fourier transform infrared (FT-IR) spectra of the membrane was obtained using a Thermo-Fisher Nicolet instrument to detect any evidence of membrane degradation.

Synthesis and characterization of ED-RFB electrolytes

The electrolytes used in this study consist of 0.9 M $VOSO_4$ in 5.8 M CH_3SO_3H and 0.9 M $Ce(CH_3SO_3)_3$ in 4 M CH_3SO_3H. $VOSO_4$ (97%, Sigma-Aldrich) was readily soluble in water and CH_3SO_3H (99%, Acros Organics) to yield the desired electrolyte. The $Ce(CH_3SO_3)_3$ was made by the reaction between CH_3SO_3H and $Ce_2(CO_3)_3$ (99%, Treibacher Industrie A.G.)-

$$Ce_2(CO_3)_3 + 6CH_3SO_3H \rightarrow 2Ce(CH_3SO_3)_3 + 3CO_2 + 3H_2O$$

The $Ce_2(CO_3)_3$ was suspended in DI water and CH_3SO_3H was added dropwise with constant stirring. Due to the sensitivity of $Ce(CH_3SO_3)_3$ solubility to the CH_3SO_3H concentration, the reaction mixture was diluted periodically with DI water to prevent precipitation of $Ce(CH_3SO_3)_3$. The $VOSO_4$ electrolyte was converted to its V^{3+} form using a symmetric V/V cell before testing the V-Ce ED-RFB.

The electrolytes were electrochemically characterized using cyclic voltammetry. The electrochemical measurements were carried out in a small-volume electrochemical cell (Pine Instruments, RRPG223) with a 3 mm diameter glassy carbon (GC) disc working electrode, a counter electrode consisting of a Pt mesh attached to a Pt wire and an Ag/AgCl reference electrode (0.197 V vs. SHE). All potentials are reported on the standard hydrogen electrode (SHE) scale unless otherwise noted. The electrochemical measurements were performed using a Solartron multichannel potentiostat.

ED-RFB tests

The ED-RFB testing was carried out using a Scribner Inc. 857 RFB test stand. The cell used was of the standard plate-and-frame configuration with a 25 cm^2 active area. The electrodes employed were made of carbon felt (SigraCELL GFA6, SGL carbon) which were activated by heating in air in a muffle furnace at 400 ℃. All tests were carried out using interdigitated flow

fields at a flow rate of 100 mL.min^{-1} and at 25 ℃. The polarization measurements were carried out by potentiostatic charging of the ED-RFB to the voltage corresponding to the desired state of charge (SOC) and then employing a current stair-step protocol with a hold time of 30 s to allow for equilibration after each step increase. After each 30 s hold, an equal and opposite current was applied so as to prevent any change in the initial SOC. The charge-discharge cycling was carried out galvanostatically between 2 V and 0.65 V at four different current densities – 25 mA.cm^{-2}, 50 mA.cm^{-2}, 75 mA.cm^{-2}, and 100 mA.cm^{-2}. The various efficiencies of the ED-RFB were calculated using the following relationships –

$$Coulombic\ efficiency\ (CE) = \frac{\text{volumetric discharge capacity } (\text{Ah.L}^{-1})}{\text{volumetric charge capacity } (\text{Ah.L}^{-1})}\ x\ 100 \qquad (4)$$

$$Energy\ efficiency\ (EE) = \frac{energy\ discharged\ (Wh.L^{-1})}{energy\ supplied\ upon\ charging\ (Wh.L^{-1})}\ x\ 100 \qquad (5)$$

The cation cross-over across the AEM separator following ED-RFB cycling was measured using a PerkinElmer Optima 7300DV inductive-coupled plasma optical emission spectrometer (ICP-OES).

Results and Discussion

The chloromethylated-SEBS-30 functionalized with trimethylamine (here after referred to as CM-SEBS-30-TMA) AEMs were successfully prepared as described in our previous reports[26,35]. The properties of these membranes are provided in **Table S1** of the **ESI**. Following the chloromethylation reaction, a degree of functionalization of 0.16 was achieved against a possible theoretical maximum of 0.3 (with all the styrene groups functionalized) as seen from the ^{1}H NMR in **ESI Figure S1**. Upon addition of the trimethylamine cation, the ion exchange capacity

was 1.35±0.02 (~90% of theoretical). The addition of TMA was confirmed by the C-N stretch in the FTIR spectra of CM-SEBS-30-TMA which was absent in spectra of CM-SEBS-30 prior to TMA addition (FTIR spectra depicted in **ESI Figure S2**). The uniform addition of TMA across the membrane was confirmed by EDAX spectral mapping obtained across the cross-section of the membrane, which showed the presence of the Cl^- counterion to TMA^+ and is depicted in **ESI Figure S3**. The ionic conductivity of the AEM was measured using a standard 4-electrode cell[36]. The AEM was ion exchanged to the sulfate and methanesulfonate form by immersion in 0.1 M H_2SO_4 and 0.1 M CH_3SO_3H respectively for 24 hours. The sulfate ion conductivity values (depicted in **Figure 2(a)**) were found to be higher than the values for the methanesulfonate anion due to the relatively smaller hydrodynamic radius of the sulfate anion[37]. The result of the AEM stability test is depicted in **Figure 2(b)**. The CM-SEBS-30-TMA AEM was found to stable over the course of this test and exhibited minimal changes in ionic conductivity and IEC. The AEM separator was found to be both thermally and mechanically robust with thermal degradation starting at over 200°C (**ESI Figure S3**), while the ultimate tensile strength was found to be 3.1±0.6 MPa.

The electrolytes used in this study were initially characterized using cyclic voltammetry as depicted in **Figure 3**. The voltammetric properties are summarized in **Table 1**. Given that the electrolytes consisted of the cations of interest in one oxidation state at the onset, cations that are formed in the other oxidation state rapidly diffuse into the bulk of the electrolyte due to the sharp concentration gradient. Thus, the CVs were recorded at a high scan rate to reduce (or oxidize) the produced redox species before it diffused away from the near electrode environment. The cathodic peaks was the lowest current density value during the negative going (cathodic) scan and the corresponding potential was recorded as the cathodic peak potential (E_c). Similarly, the anodic

peak was the highest current density value during the positive going (anodic) scan and the corresponding potential was recorded as the anodic peak potential (E_a). The difference between E_c and E_a was the peak separation (ΔE_p). The peak separation (ΔE_p) for the V^{2+}/V^{3+} redox couple was found to be 1.43 V while the peak separation for the Ce^{3+}/Ce^{4+} redox couple was found to be 0.64V, which indicated irreversibility. The formal potential (E_{form}) values were calculated as $E_{form} = (E_c + E_a)/2$. Based on the formal potential, the cathodic and anodic half-wave potentials (i.e. potential where the anodic (or cathodic) current is one-half the peak value) $E_{c/2}$ and $E_{a/2}$ were calculated. E_{form} showed significant deviation from the E^0 values (270 mV for the V^{2+}/V^{3+} redox couple and 500 mV for the Ce^{3+}/Ce^{4+} redox couple) indicating the strong effect of the $CH_3SO_3^-$ ion coordination with the redox species. E_{form} cannot be directly correlated to E_0 as E_0 is an ideal value at equal concentrations of the reduced and oxidized species, without accounting for the effects of the supporting electrolyte. The comparison between the two is intended to highlight the solvating effect of the $CH_3SO_3^-$ anion. This effect has been documented in case of the Ce^{3+}/Ce^{4+} redox couple[38] and a similar mechanism appears to apply in case of the V^{2+}/V^{3+} redox couple. A further consideration for the V^{2+}/V^{3+} redox couple is that use of the $VOSO_4$ salt will ensure that the V^{2+}/V^{3+} redox couple is coordinated with both SO_4^{2-} and CH_3SO_3H anions. Thus, the CV characteristics are a function of this coordination structure. The effect of the solvation structure on these redox couples was characterized by calculating the solvent reorganization energy (λ). λ is the amount of energy required to rearrange the reactant solvation shell to its product form and plays a prominent role in the Marcus-Hush kinetic formulation for heterogenous electron transfer processes[39,40]. λ was calculated using the following equation given by Saveant *et al*[41]:

$$\alpha = 0.5 + \frac{F}{4\lambda}(E - E^0 - \phi_r) \quad (6)$$

Here, α is the transfer coefficient, F is the Faraday's constant (96485 C/mol of e^-), ϕ_r is the potential at the plane of the reaction site vs. bulk solution and E^0 is the standard potential of the electrochemical reaction under consideration. The reactions were assumed to occur every close to the electrode surface and hence $\phi_r \approx$ E.

Since the electrolytes initially consist of V^{3+} and Ce^{3+} respectively, only the cathodic reaction of the V^{2+}/V^{3+} redox couple and the anodic reaction of the Ce^{3+}/Ce^{4+} redox couple were examined. This limitation is due to the local concentration of V^{2+} and Ce^{4+} being unknown and the scan rate dependence of the oxidation and reduction currents respectively of these two species (due to the outward diffusion of the products into the bulk electrolyte). The transfer coefficients (listed in **Table 1**) were calculated using the following equation[42]:

$$\alpha = \frac{1.86RT}{F\left(E_P - E_{\frac{P}{2}}\right)} \quad (7)$$

Where, R is the universal gas constant (8.314 J mol^{-1} K^{-1}), T is the temperature (298 K) and E_p and $E_{P/2}$ are the peak and half-peak potentials respectively of the anodic or cathodic reaction. The α typically has a value of 0.5 which indicates that the anodic and cathodic reactions are equally facile and the occurrence of either is a function of the applied overpotential. The values of 0.2 for the $V^{3+} + e^- \rightarrow V^{2+}$ reaction and 0.3 for the $Ce^{3+} \rightarrow Ce^{4+} + e^-$ reaction indicated that forward and backward reactions are not equally facile, supporting the inference of an irreversible reaction from the >60 mV peak separation in the CVs. Assuming the overall reactions for both couples are one-step and one-electron transfer, we have $\alpha_c + \alpha_a = 1$[43] and the transfer coefficient for the $V^{2+} \rightarrow V^{3+} + e^-$ reaction is 0.8 and the $Ce^{4+} + e^- \rightarrow Ce^{3+}$ reaction has a transfer coefficient of 0.7. **Figure**

3(b) depicts the Tafel analysis carried out on the $V^{3+} + e^- \rightarrow V^{2+}$ and $Ce^{3+} \rightarrow Ce^{4+} + e^-$ reactions. The Tafel equation is as follows[44]:

$$\eta = a + b.\log\,(i_k) \tag{8}$$

Where,

$$a = \frac{2.3RT}{\alpha.F}.logi_0 \tag{9}$$

$$b = -\frac{2.3RT}{\alpha.F} \tag{10}$$

Here, i_0 is the exchange current density in mA cm^{-2}. The value of the Tafel slope for a one electron transfer reaction with the $\alpha = 0.5$ would be 118 mV dec^{-1}. In case of the reactions considered here, $\alpha_c = 0.2$ would result in a cathodic Tafel slope of 295 mV dec^{-1}, while $\alpha_a = 0.3$ would result in an anodic Tafel slope of 197 mV dec^{-1} while the measured values were 210 mV dec^{-1} and 140 mV dec^{-1} respectively. The deviations were the result of experimental noise and the lack of an adequate linear region in the Tafel plots. The Tafel slopes and the measured i_0 for the Ce^{3+}/Ce^{4+} redox couple were found to broadly agree with a report by Nikiforidis *et al.*[45].

The polarization characteristics of the V-Ce ED-RFB measured at 20% and 60% SOC are depicted in **Figure 4**. Before polarization measurements, the OCV was monitored at 0% SOC and found to be 1.337 V as compared to the 2.09 V difference in E_{form} from the CVs and the theoretical value of 1.87 V. Substantial activation losses (at 10 mA.cm^{-2}) of 310 mV and 320 mV were observed at 20% and 60% SOC respectively during discharge while the charging activation losses were 152 mV and 116 mV respectively for 20% and 60% SOC. This was consistent with the irreversible nature of the CVs and the large reduction and oxidation overpotentials. The

optimization of the carbon felt heat treatment process[46], the use of chemical treatments such as immersion in *aqua regia*[47] or the use of catalysts could alleviate this issue. Distinct asymmetry was observed over the charge and discharge branches of the polarization curve with the average resistance during discharge being 0.54 Ω while the average charge resistance was 0.15 Ω. A part of this resistance is ohmic and the *ex-situ* membrane area specific resistance (ASR) of 0.51 $\Omega.cm^2$ (σ_{IP} = 11.69 $mS.cm^{-1}$ for a 60 μm thick membrane) suggested that these losses can be partially mitigated through improved membrane ionic conductivity. The ohmic losses would necessarily be symmetric and thus, the asymmetry was attributed to the highly irreversible nature of the half-cell reactions. The voltage profiles showed no mass-transport losses, indicating that the 100 $mL.min^{-1}$ flowrates employed was sufficient to prevent active species depletion near the electrode to a current of *ca*. 200 $mA.cm^{-2}$. The absence of mass-transport losses may also be attributed to the use of interdigitated flow fields, as they have been shown to substantially improve the flow distribution through and over the surface of the porous electrode[48–50].

Figure 5(a) depicts the impact of separator and supporting electrolyte selection on ED-RFB performance. The use of Nafion® is impractical as it readily allows the mixing of the cations and hence does not allow an "electrode-decoupled" RFB architecture. The resultant capacity loss due to electrolyte mixing was apparent in the very first cycle and resulted in >40% capacity fade in 20 cycles at 50 $mA.cm^{-2}$ as demonstrated previously[26]. The first cycle capacity difference between the other two RFBs utilizing the same CM-SEBS-30-TMA AEM separator was attributed to the increase in concentration achieved by using CH_3SO_3H as the supporting electrolyte. **Figure 5(b)** depicts the impact of increasing current density on the achievable capacity in the CH_3SO_3H supported V-Ce ED-RFBs. The decline in available discharge capacity followed a typical direct correlation with the current density. The absolute values of achievable capacity can be improved

by (in order of importance) improving the reversibility of the half-cell reactions, by the use of catalysts to lower activation losses, and by improving membrane conductivity.

Figure 6(a) depicts the cycling performance of the ED-RFB over 100 cycles at 50 mA.cm^{-2}. A 2.4% loss of initial capacity was observed over the course of this test which was substantially better than the ~10% capacity loss observed over 20 cycles for ED-RFB systems utilizing the same AEM separator but with the H_2SO_4 based electrolytes[26]. The membranes used in Wang *et. al.* and this study were nearly identical in terms of properties. Thus, the substantially improved capacity retention is a direct result of the CH_3SO_3H supporting electrolyte and the resultant changes in the cation solvation. Significantly, while the increase in cation concentration resulted in a sharper concentration gradient across the separator (and hence could increase cross-over), the increased hydrodynamic radius of the $CH_3SO_3^-$ anions compared to SO_4^{2-} (as inferred from the ionic conductivity values) and the corresponding increase in the radii of the $CH_3SO_3^-$solvated cations would also lead to a size exclusion effect that decreases cross-over. The improved capacity and capacity retention indicates that the solvation effect negates the increased concentration gradient. Assuming the capacity fade is caused only by the cation cross-over route and given that the redox processes are 1-electron transfer processes at both electrodes, it can be inferred that 2.4% (0.0216 moles) of the initial cation concentration on one side was transferred to the other. ICP-OES analysis of the electrolytes after cycling indicated that 0.017 moles of the cation has crossed-over, closely correlating with the capacity fade. These ED-RFBs also demonstrated an average EE of 65% over the course of the 100 cycles with a 6% decline over that period which was again a substantial improvement over the 12% loss over 20 cycles with the H_2SO_4 based V-Ce ED-RFB[26]. **Figure 6(b)** shows the impact of charge/discharge currents on the energy efficiency and coulombic efficiency of the ED-RFB. Even at 100 mA.cm^{-2}, EE of >50% was achieved. Further, even after

relatively high current charge-discharge cycles, upon cycling again at 50 mA.cm-2, the ED-RFB EE was found to return to the values initially recorded at 50 mA.cm^{-2}. This indicated that the cell was experiencing minimal side- or parasitic reactions.

The key to long-term use of this ED-RFB configuration in the field is the chemical stability and sustained selectivity of the separator. The sustained selectivity of the CM-SEBS-30-TMA separators has been demonstrated by the minimal capacity fade achieved over long-term cycling. The chemical stability of these separators was examined by looking for evidence of loss of the functionalizing cation. Mohanty *et al.*[51] showed using FT-IR spectroscopy that the C-N stretch characteristic of the TMA^+ cation could be used to verify the stability of the CM-SEBS-30-TMA AEM. As seen in **Figure 7**, the C-N stretch is evident in both the pristine membrane and the membrane after long-term cycling indicating no loss of the TMA^+ cation. The apparent loss in intensity was not evidence of AEM degradation as the ratio between the C=C bend and C-N stretch remained constant. To rule out other degradation routes, the Cl^- conductivity of the membrane before and after ED-RFB testing was measured. The conductivity showed no decline within experimental error, indicating no membrane degradation within the ~150-hour duration of the experiments as depicted in **Figure 8**. Thus, the CM-SEBS-30-TMA AEM separator was found to be chemically stable over the course of long-term cycling.

Conclusions

An electrode-decoupled redox flow battery with excellent energy efficiency, long cycle life and environmentally friendly electrolyte formulation has been demonstrated. The change in cation solvation structure (compared to H_2SO_4 based electrolytes) brought about by the use of CH_3SO_3H greatly improved separator selectivity. In summary, the 30% improvement in capacity, 2.4%

capacity fade over 100 cycles and ~70% energy efficiency demonstrated by the methanesulfonic-acid-based V-Ce ED-RFB makes it an excellent candidate for various energy storage applications. The demonstrated capacity retention and fast response times of the ED-RFB enables its application in frequency regulation and demand-response when coupled with an intermittent power source (such as solar or wind) while the modular nature and sub-linear cost scaling enable applications in weak grid and off-grid energy storage applications[52,53].

Acknowledgements

The authors gratefully acknowledge financial support from the Advanced Research Projects Agency-Energy (ARPA-E), the US Department of Energy under award no. DE-AR0000768 as part of the Integration and Optimization of Novel Ion Conducting Solids (IONICS) program. The authors acknowledge with gratitude the McKelvey School of Engineering and Applied Sciences, Washington University in St. Louis and the Roma B. & Raymond H. Wittcoff Distinguished University Professorship. The authors thank the High-Resolution NMR Facility, Department of Chemistry at Washington University in St. Louis for access to the ^{1}H-NMR. The FT-IR spectroscopy and electron microscopy reported in this work was performed at the Nano Research Facility (NRF), a member of the National Nanotechnology Infrastructure Network (NNIN), which is supported by the National Science Foundation under Grant No. ECS-0335765. NRF is part of the School of Engineering and Applied Science at Washington University in St. Louis. The authors declare no conflict of interest.

References

1 Department of Energy, Funding Opportunity Announcement Advanced Research Projects Agency – Energy (Arpa-E) Duration Addition to Electricity Storage (DAYS), *DE-FOA-*

0001906.

2 U.S Energy Information Administration, Levelized Cost and Levelized Avoided Cost of New Generation Resources in the Annual Energy Outlook 2018, https://www.eia.gov/outlooks/aeo/pdf/electricity_generation.pdf.

3 G. L. Soloveichik, Flow Batteries: Current Status and Trends, *Chem. Rev.*, 2015, **115**, 11533–11558.

4 R. Dmello, J. D. Milshtein, F. R. Brushett and K. C. Smith, Cost-driven materials selection criteria for redox flow battery electrolytes, *J. Power Sources*, 2016, **330**, 261–272.

5 R. M. Darling, K. G. Gallagher, J. A. Kowalski, S. Ha and F. R. Brushett, Pathways to low-cost electrochemical energy storage: a comparison of aqueous and nonaqueous flow batteries, *Energy Environ. Sci.*, 2014, **7**, 3459–3477.

6 P. S. Fedkiw and R. W. Watts, A mathematical model for the iron/chromium redox battery, *J. Electrochem. Soc.*, 1984, **131**, 701–709.

7 V. Jalan, B. Morriseau and L. Swette, Optimization and fabrication of porous carbon electrodes for Fe/Cr redox flow cells, *Nasa Cr-167921*.

8 R. F. Gahn, N. H. Hagedorn and J. A. Johnson, Cycling Performace of the Iron-Chromium Redox Energy Storage System Conservation and Renewable Energy, *Nasa Tm-87034*.

9 M. Rychcik and M. Skyllas-Kazacos, Characteristics of a new all-vanadium redox flow battery, *J. Power Sources*, 1988, **22**, 59–67.

10 M. Ulaganathan, V. Aravindan, Q. Yan, S. Madhavi, M. Skyllas-Kazacos and T. M. Lim, Recent Advancements in All-Vanadium Redox Flow Batteries, *Adv. Mater. Interfaces*, 2016, **3**, 1–22.

11 P. K. Leung, C. Ponce-De-Le??n, C. T. J. Low, A. A. Shah and F. C. Walsh, Characterization of a zinc-cerium flow battery, *J. Power Sources*, 2011, **196**, 5174–5185.

12 P. K. Leung, C. Ponce De León and F. C. Walsh, An undivided zinc-cerium redox flow battery operating at room temperature (295 K), *Electrochem. commun.*, 2011, **13**, 770–773.

13 K. Leung, Two-electron reduction of ethylene carbonate: A quantum chemistry re-examination of mechanisms, *Chem. Phys. Lett.*, 2013, **568**–**569**, 1–8.

14 K. L. Hawthorne, J. S. Wainright and R. F. Savinell, Studies of Iron-Ligand Complexes for an All-Iron Flow Battery Application, *J. Electrochem. Soc.*, 2014, **161**, A1662–A1671.

15 K. Gong, F. Xu, J. B. Grunewald, X. Ma, Y. Zhao, S. Gu and Y. Yan, All-Soluble All-Iron Aqueous Redox-Flow Battery, *ACS Energy Lett.*, 2016, **1**, 89–93.

16 K. Lin, R. Gómez-Bombarelli, E. S. Beh, L. Tong, Q. Chen, A. Valle, A. Aspuru-Guzik, M. J. Aziz and R. G. Gordon, A redox-flow battery with an alloxazine-based organic electrolyte, *Nat. Energy*, 2016, **1**, 16102.

17 E. S. Beh, D. De Porcellinis, R. L. Gracia, K. T. Xia, R. G. Gordon and M. J. Aziz, A Neutral pH Aqueous Organic–Organometallic Redox Flow Battery with Extremely High Capacity Retention, *ACS Energy Lett.*, 2017, **2**, 639–644.

18 B. Yang, L. Hoober-Burkhardt, S. Krishnamoorthy, A. Murali, G. K. S. Prakash and S. R.

Narayanan, High-Performance Aqueous Organic Flow Battery with Quinone-Based Redox Couples at Both Electrodes, *J. Electrochem. Soc.*, 2016, **163**, A1442–A1449.

19 J. D. Milshtein, L. Su, C. Liou, A. F. Badel and F. R. Brushett, Voltammetry study of quinoxaline in aqueous electrolytes, *Electrochim. Acta*, 2015, **180**, 695–704.

20 F. R. Brushett, J. T. Vaughey and A. N. Jansen, An all-organic non-aqueous lithium-ion redox flow battery, *Adv. Energy Mater.*, 2012, **2**, 1390–1396.

21 Q. Liu, A. A. Shinkle, Y. Li, C. W. Monroe, L. T. Thompson and A. E. S. Sleightholme, Non-aqueous chromium acetylacetonate electrolyte for redox flow batteries, *Electrochem. commun.*, 2010, **12**, 1634–1637.

22 A. E. S. Sleightholme, A. A. Shinkle, Q. Liu, Y. Li, C. W. Monroe and L. T. Thompson, Non-aqueous manganese acetylacetonate electrolyte for redox flow batteries, *J. Power Sources*, 2011, **196**, 5742–5745.

23 I. L. Escalante-Garcia, J. S. Wainright, L. T. Thompson and R. F. Savinell, Performance of a Non-Aqueous Vanadium Acetylacetonate Prototype Redox Flow Battery: Examination of Separators and Capacity Decay, *J. Electrochem. Soc.*, 2014, **162**, A363–A372.

24 D. Chen and M. A. Hickner, V5+ degradation of sulfonated Radel membranes for vanadium redox flow batteries, *Phys. Chem. Chem. Phys.*, 2013, **15**, 11299–11305.

25 S. Yun, J. Parrondo and V. Ramani, A vanadium-cerium redox flow battery with an anion-exchange membrane separator, *Chempluschem*, 2015, **80**, 412–421.

26 Z. Wang, J. Parrondo and V. Ramani, Polystyrene-Block-Poly(ethylene-ran-butylene)-

Block-Polystyrene Triblock Copolymer Separators for a Vanadium-Cerium Redox Flow Battery, *J. Electrochem. Soc.*, 2017, **164**, 372–378.

27 R. P. Kreh, R. M. Spotnitz and J. T. Lundquist, Mediated Electrochemical Synthesis of Aromatic Aldehydes, Ketones, and Quinones Using Ceric Methanesulfonate, *J. Org. Chem.*, 1989, **54**, 1526–1531.

28 J. G. Speight, *Lange ' S Handbook of Chemistry*, 2005.

29 P. K. Leung, C. Ponce De León, C. T. J. Low and F. C. Walsh, Ce(III)/Ce(IV) in methanesulfonic acid as the positive half cell of a redox flow battery, *Electrochim. Acta*, 2011, **56**, 2145–2153.

30 L. F. Arenas, C. Ponce de León and F. C. Walsh, Pressure drop through platinized titanium porous electrodes for cerium-based redox flow batteries, *AIChE J.*, 2018, **64**, 1135–1146.

31 Z. Na, S. Xu, D. Yin and L. Wang, A cerium–lead redox flow battery system employing supporting electrolyte of methanesulfonic acid, *J. Power Sources*, 2015, **295**, 28–32.

32 P. K. Leung, M. R. Mohamed, A. A. Shah, Q. Xu and M. B. Conde-Duran, A mixed acid based vanadium–cerium redox flow battery with a zero-gap serpentine architecture, *J. Power Sources*, 2015, **274**, 651–658.

33 M. Govindan, K. He and I. S. Moon, Evaluation of dual electrochemical cell design for cerium-vanadium redox flow battery to use different combination of electrodes, *Int. J. Electrochem. Sci.*, 2013, **8**, 10265–10279.

34 M. D. Gernon, M. Wu, T. Buszta and P. Janney, Environmental benefits of

methanesulfonic acid, *Green Chem.*, 1999, **1**, 127–140.

35 Z. Wang, J. Parrondo and V. Ramani, Anion Exchange Membranes Based on Polystyrene-*Block* -Poly(ethylene- *ran* -butylene)- *Block* -Polystyrene Triblock Copolymers: Cation Stability and Fuel Cell Performance, *J. Electrochem. Soc.*, 2017, **164**, F1216–F1225.

36 K. R. Cooper, Characterizing Through-Plane and In-plane Ionic Conductivity of Polymer Electrolyte Membranes, *ECS Trans.*, 2011, **41**, 1371–1380.

37 J. R. Varcoe, P. Atanassov, D. R. Dekel, A. M. Herring, M. A. Hickner, P. A. Kohl, A. R. Kucernak, W. E. Mustain, K. Nijmeijer, K. Scott, T. Xu and L. Zhuang, Anion-exchange membranes in electrochemical energy systems, *Energy Environ. Sci.*, 2014, **7**, 3135–3191.

38 P. K. Leung, C. Ponce De León, C. T. J. Low and F. C. Walsh, Ce(III)/Ce(IV) in methanesulfonic acid as the positive half cell of a redox flow battery, *Electrochim. Acta*, 2011, **56**, 2145–2153.

39 P. Bai and M. Z. Bazant, Charge transfer kinetics at the solid-solid interface in porous electrodes, *Nat. Commun.*, 2014, **5**, 1–7.

40 E. Laborda, M. C. Henstridge, C. Batchelor-Mc Auley and R. G. Compton, Asymmetric marcus–Hush theory for voltammetry, *Chem. Soc. Rev.*, 2013, **42**, 4894–4905.

41 J.-M. Savéant and D. Tessier, Potential dependence of the electrochemical transfer coefficient. Reduction of some nitro compounds in aprotic media, *J. Phys. Chem.*, 1977, **81**, 2192–2197.

42 C. O. Laoire, S. Mukerjee, K. M. Abraham, E. J. Plichta and M. A. Hendrickson, Influence of nonaqueous solvents on the electrochemistry of oxygen in the rechargeable

lithium-air battery, *J. Phys. Chem. C*, 2010, **114**, 9178–9186.

43 J. O. ' M. Bockris and Z. Nagy, *J. Chem. Educ.*, 1973, 50, 839.

44 A. J. Bard and L. R. Faulkner, *Electrochemical Methods: Fundamentals and Applications*, Wiley, 2nd edn., 2000.

45 G. Nikiforidis, L. Berlouis, D. Hall and D. Hodgson, An electrochemical study on the positive electrode side of the zinc-cerium hybrid redox flow battery, *Electrochim. Acta*, 2013, **115**, 621–629.

46 K. V. Greco, A. Forner-Cuenca, A. Mularczyk, J. J. Eller and F. R. Brushett, Elucidating the Nuanced Effects of Thermal Pretreatment on Carbon Paper Electrodes for Vanadium Redox Flow Batteries, *ACS Appl. Mater. Interfaces*, 2018, acsami.8b15793.

47 Y. K. K. Zeng, X. L. L. Zhou, L. An, L. Wei and T. S. S. Zhao, A high-performance flow-field structured iron-chromium redox flow battery, *J. Power Sources*, 2016, **324**, 738–744.

48 J. Houser, A. Pezeshki, J. T. Clement, D. Aaron and M. M. Mench, Architecture for improved mass transport and system performance in redox flow batteries, *J. Power Sources*, 2017, **351**, 96–105.

49 X. Ke, J. M. Prahl, J. I. D. Alexander and R. F. Savinell, Redox flow batteries with serpentine flow fields: Distributions of electrolyte flow reactant penetration into the porous carbon electrodes and effects on performance, *J. Power Sources*, 2018, **384**, 295–302.

50 Y. K. Zeng, X. L. Zhou, L. Zeng, X. H. Yan and T. S. Zhao, Performance enhancement of iron-chromium redox flow batteries by employing interdigitated flow fields, *J. Power*

Sources, 2016, **327**, 258–264.

51 A. D. Mohanty, C. Y. Ryu, Y. S. Kim and C. Bae, Stable Elastomeric Anion Exchange Membranes Based on Quaternary Ammonium-Tethered Polystyrene-b-poly(ethylene-co-butylene)-b-polystyrene Triblock Copolymers, *Macromolecules*, 2015, **48**, 7085–7095.

52 Z. Yang, J. Zhang, M. C. W. Kintner-Meyer, X. Lu, D. Choi, J. P. Lemmon and J. Liu, Electrochemical Energy Storage for Green Grid, *Chem. Rev.*, 2011, **111**, 3577–3613.

53 B. Dunn, H. Kamath and J. Tarascon, for the Grid : A Battery of Choices, *Science (80-.).*, 2011, **334**, 928.

Table 1. Voltammetric properties of the V^{2+}/V^{3+} and Ce^{3+}/Ce^{4+} redox couples and heterogenous charge transfer parameters calculated from the same. The locations of E_c, E_a and E_{form} are indicated in **Figure 3(a)** while the calculation of the other properties are described in text.

	V^{2+}/V^{3+} redox couple	**Ce^{3+}/Ce^{4+} redox couple**
E_c (V)	-1.25	1.24
$E_{c/2}$ (V)	-1.06	1.41
E_a (V)	0.18	1.88
$E_{a/2}$ (V)	-0.14	1.69
E_{form} (V)	-0.53	1.56
ΔE_p (V)	1.43	0.64
α	0.2 ($V^{3+} + e^- \rightarrow V^{2+}$)	0.3 ($Ce^{3+} \rightarrow Ce^{4+} + e^-$)
$\lvert\lambda\rvert$ (kJ.mol^{-1})	51000	150000
$\lvert\lambda/F\rvert$ (V)	0.53	1.54

Figure captions:

Figure 1. Schematic of an electrode-decoupled V-Ce redox flow battery. Standard redox potentials for the V^{3+}/V^{2+} and Ce^{4+}/Ce^{3+} couples are provided[28]. The solid lines depict the direction of electron and anion movement during the charging process while the dashed lines depict the discharge process.

Figure 2. (a) Temperature dependence of the sulphate and methanesulfonate ionic conductivity of CM-SEBS-30-TMA separators; **(b)** Representative SEBS separator stability in methanesulfonic acid at 40℃.

Figure 3. (a) Cyclic voltammograms of the V^{3+}/V^{2+} and Ce^{4+}/Ce^{3+} redox couples in methanesulfonic acid, W.E: 0.07 cm^2 GC disk, C.E: Pt mesh, R.E: Ag/AgCl (0.197 V vs. SHE), scan rate: 500 $mV.s^{-1}$; **(b)** Tafel plots of the charging reactions of the V-Ce ED-RFB.

Figure 4. Charge-discharge polarization curves of the V-Ce ED-RFB at 20% and 60% SOC.

Figure 5. Charge-discharge curves of the V-Ce ED-RFB **(a)** with different separators and supporting electrolytes, **(b)** at different current densities (CH_3SO_3H supporting electrolyte).

Figure 6. Performance of the CH_3SO_3H supported V-Ce ED-RFB **(a)** over 100 cycles at $50mA.cm^{-2}$, **(b)** rate capability test at different current densities.

Figure 7. FT-IR spectra of the CM-SEBS-30-TMA separator before and after the ED-RFB test.

Figure 8. In-plane membrane conductivity measurements before and after ED-RFB cycling

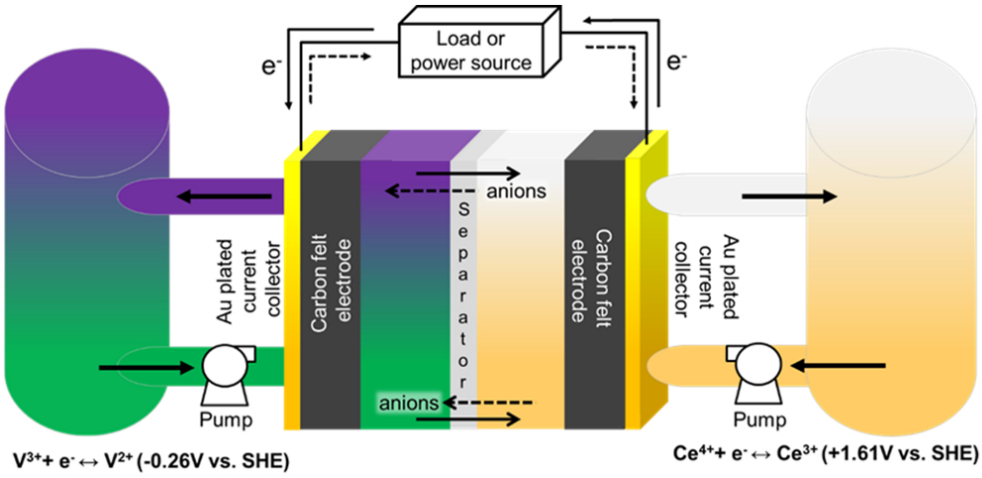

172x83mm (149 x 149 DPI)

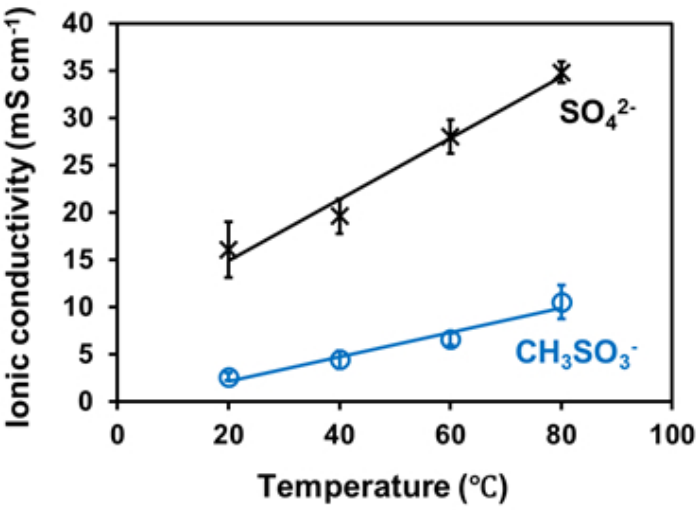

(a)

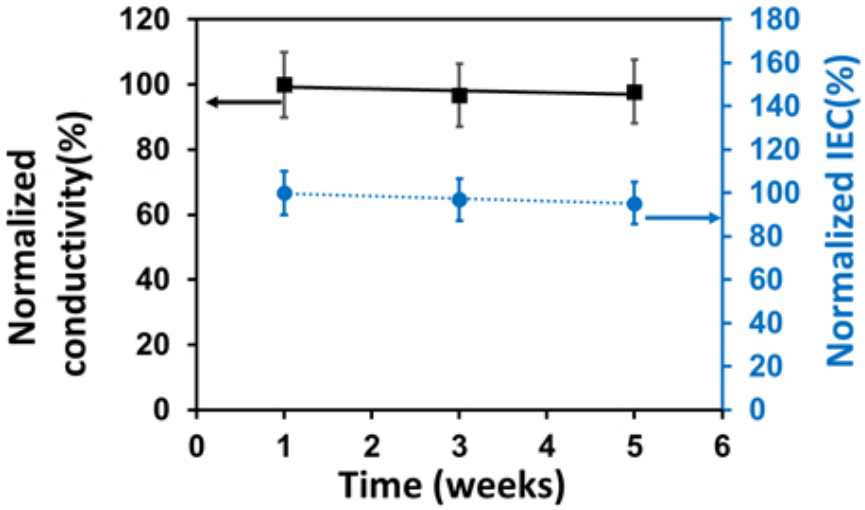

(b)

82x107mm (150 x 150 DPI)

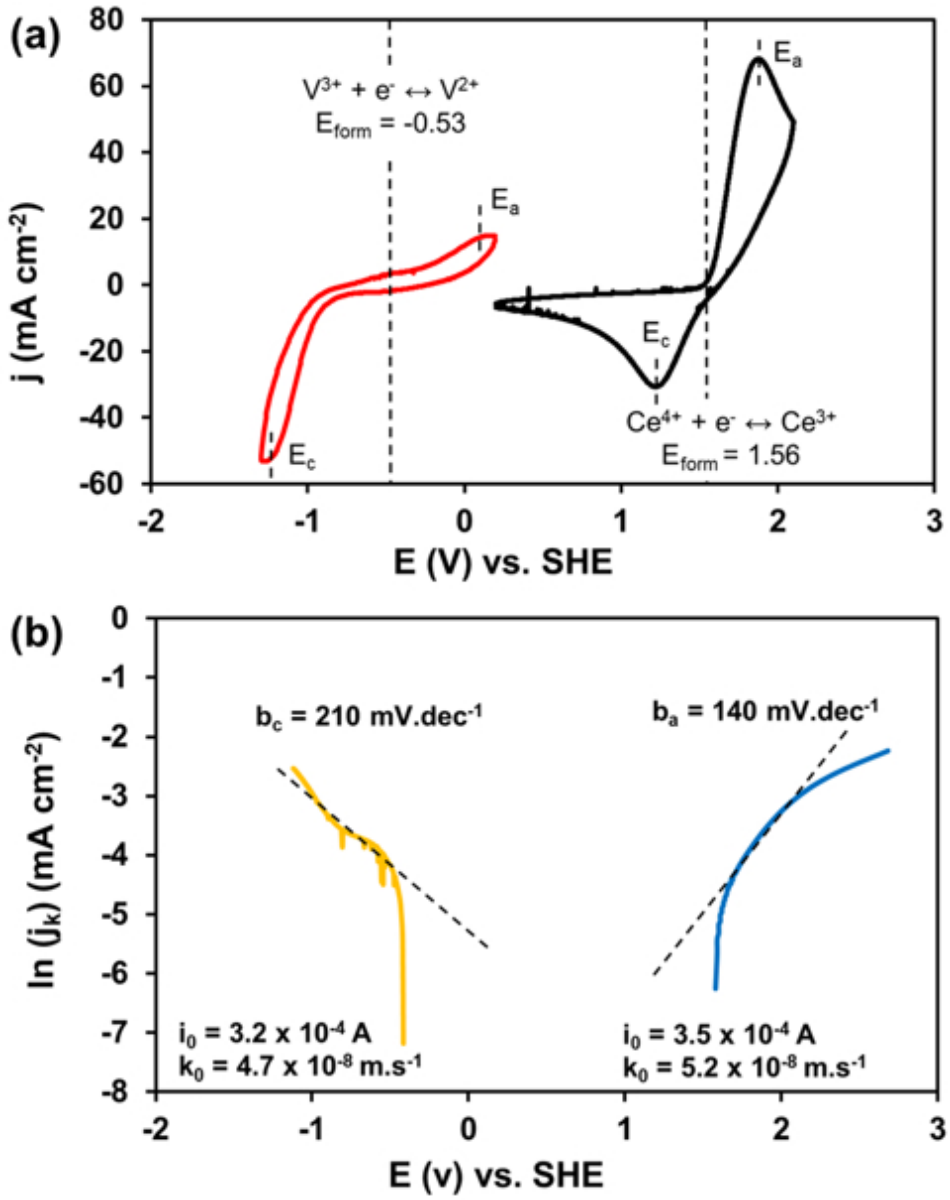

82x103mm (149 x 149 DPI)

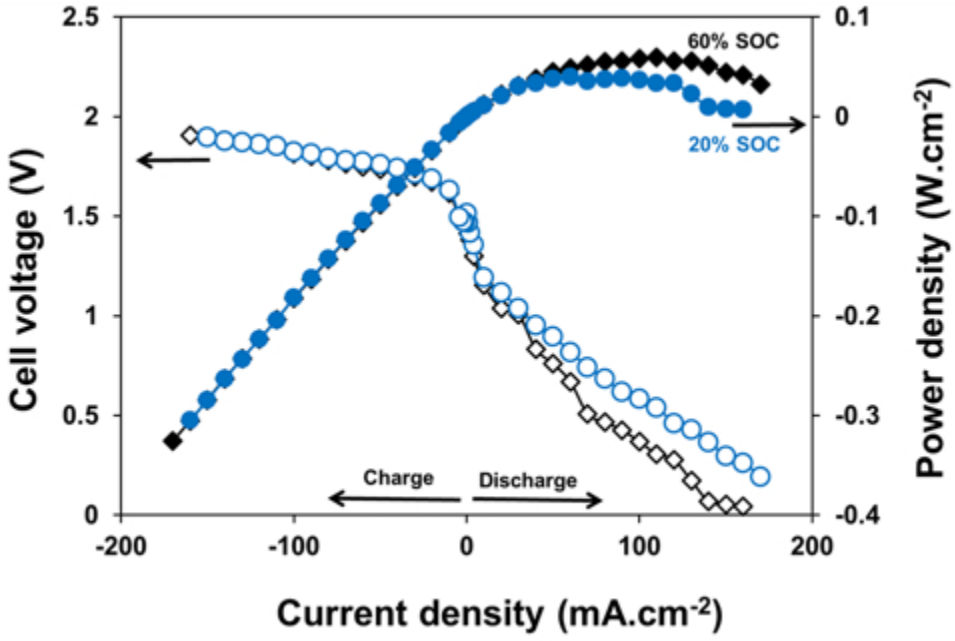

82x55mm (149 x 149 DPI)

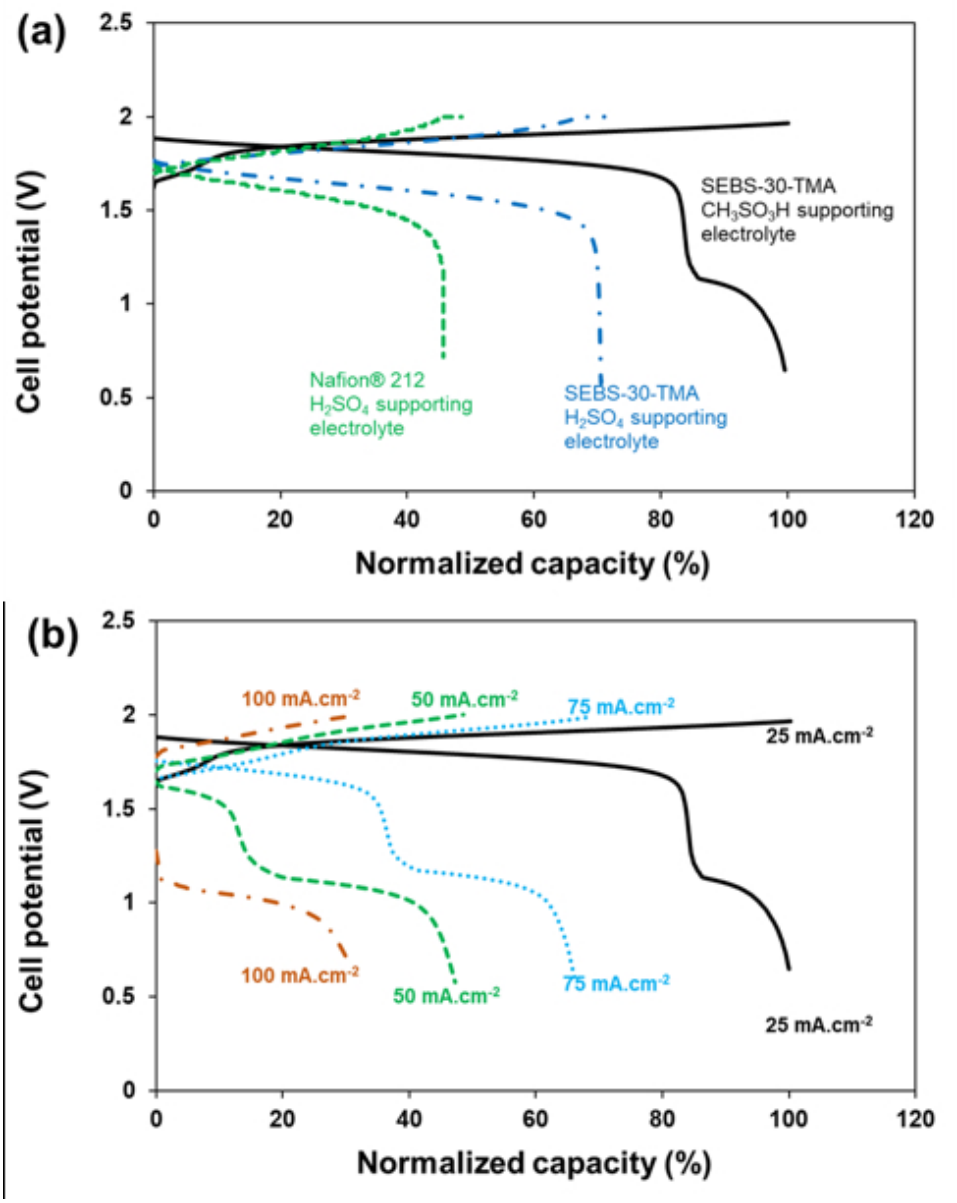

82x104mm (149 x 149 DPI)

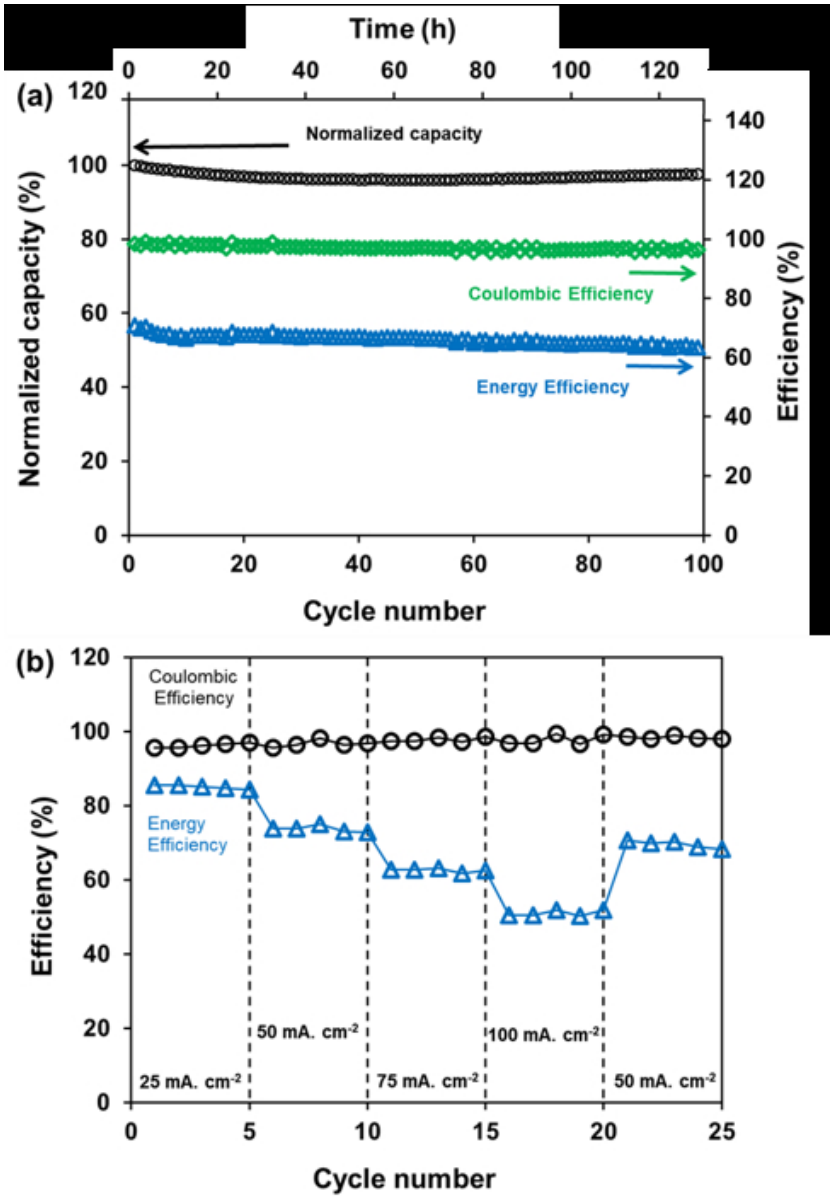

82x120mm (149 x 149 DPI)

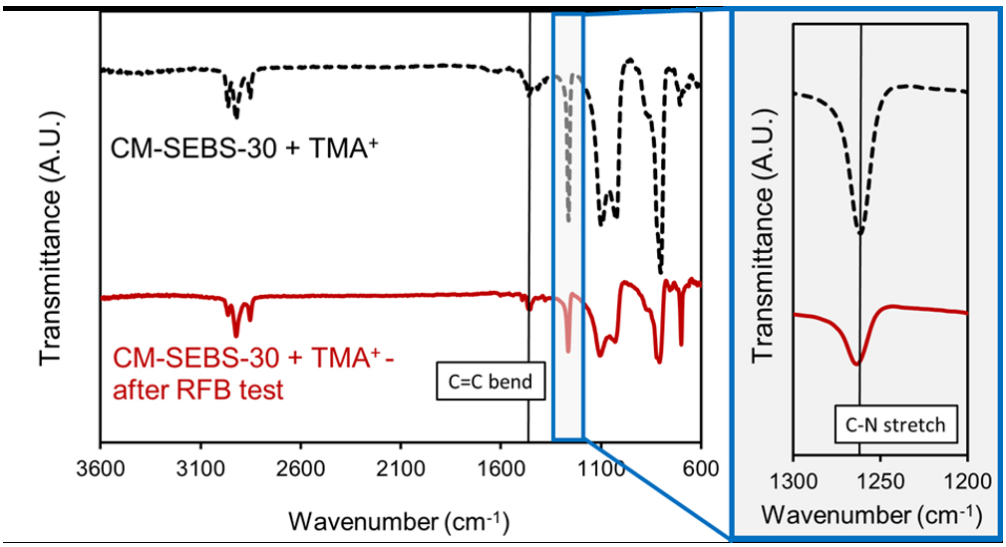

170x91mm (149 x 149 DPI)

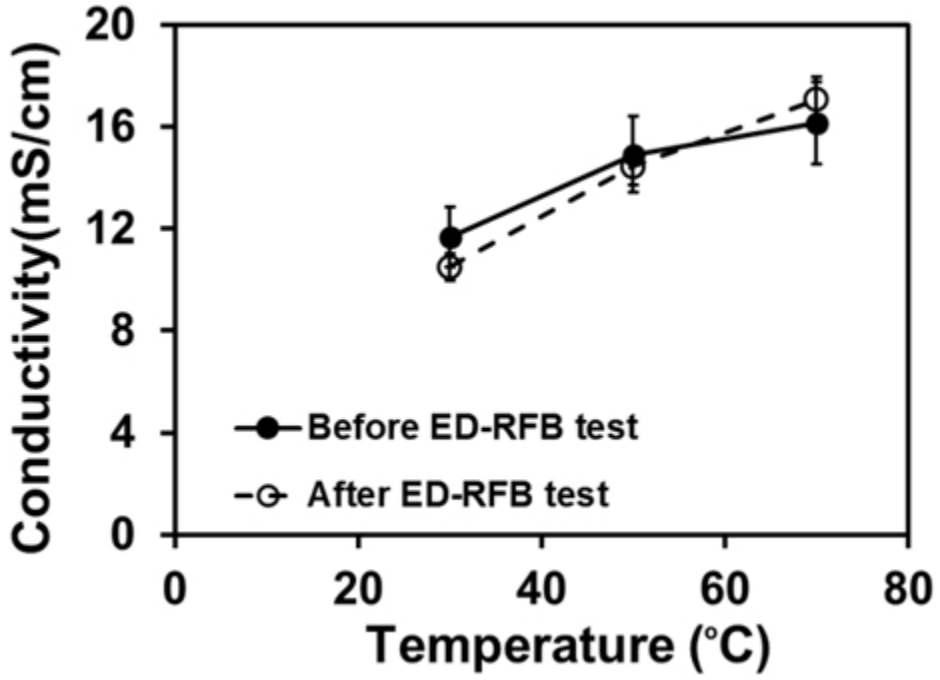

82x58mm (149 x 149 DPI)

Graphical Abstract

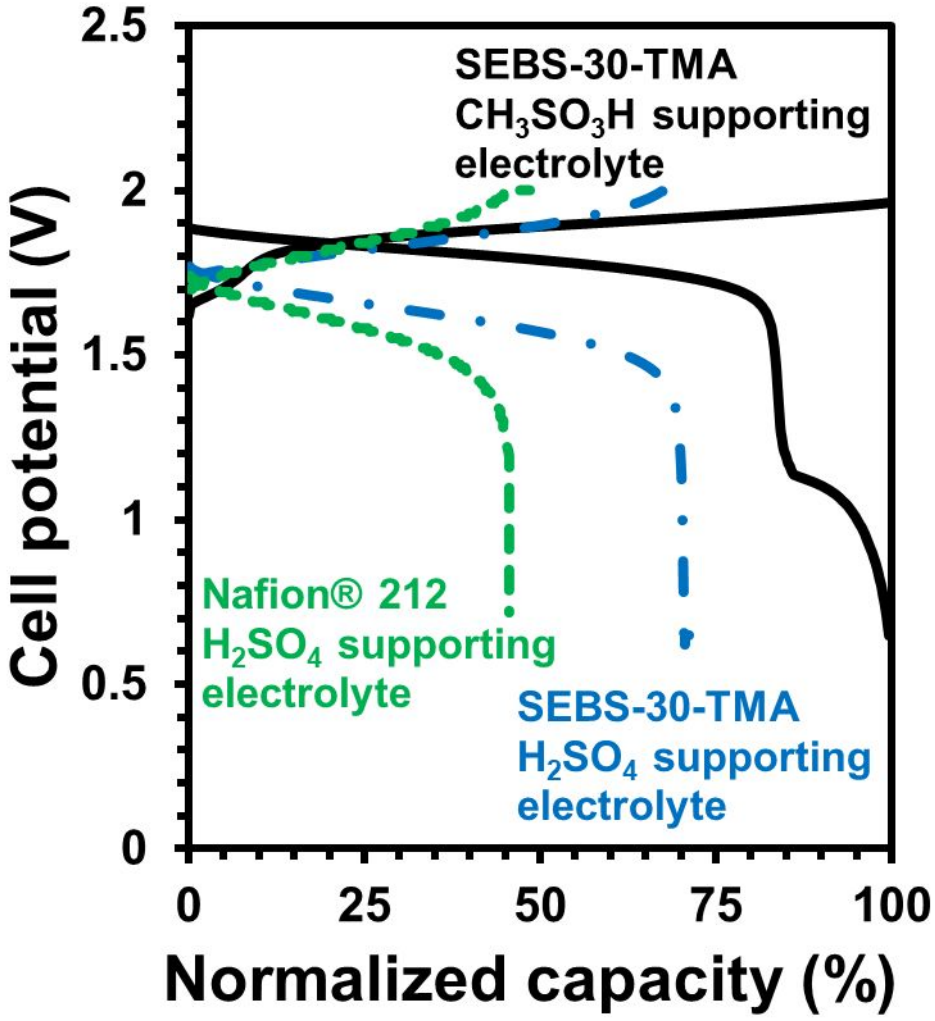

Vanadium-cerium redox flow batteries using a cerium-methanesulfonate-salt-based electrolyte and a highly permselective anion exchange separator exhibits 30% higher practical capacity and 0.024% capacity fade/ cycle compared to 5% capacity fade/ cycle for H_2SO_4 supported V-Ce ED-RFBs with ~100% coulombic efficiency (CE) and ~70% energy efficiency (EE) over 100 cycles.

Keywords: Anion-exchange membrane; Cyclic voltammetry; Energy storage; Redox-flow battery; Sustainable chemistry.